Polymer Journal, Vol. 36, No. 5, pp. 394—402 (2004)

# Orientation Distribution Functions of the Three Principal Crystallographic Axes as well as Crystallites of Poly(ethylene terephthalate) Films under Biaxially Stretching

Yuezhen BIN, Kumiko OISHI, Kyouko YOSHIDA, Teruo NAKASHIMA,* and Masaru MATSUO†

*Department of Textile and Apparel Science, Faculty of Human Life and Environment, Nara Women's University, Nara 630-8263, Japan*
**Institute of Reseach Recycling, Kinki University, 3327-240, Nakamachi, Nara 631-0052, Japan*

(Received December 10, 2003; Accepted February 6, 2004; Published May 15, 2004)

ABSTRACT: The orientation of the three principal crystallographic axes, the *a*-, *b*-, and *c*-axes of crystallites of poly(ethylene terephthalate) (PET) under simultaneous biaxial stretching was estimated in terms of the orientation distribution function. For most of crystalline polymers with a triclinic unit like PET, there are no crystal planes perpendicular to the *a*-, *b*-, and *c*-axes that can be detected directly by X-Ray diffraction techniques. Accordingly, the functions of the *a*-, *b*-, and *c*-axes must be calculated by the method proposed by Roe and Krigbaum. In doing so, the orientation functions of the reciprocal lattice vectors must be measured for a number of crystal planes. In this paper, as an example, the orientation of crystallites and the orientation of the *a*-, *b*-, and *c*-axes were estimated for a PET film under simultaneous biaxial stretching in terms of the orientation distribution function of crystallites because of considerable utilization rate of PET as commercial films. The estimated orientation functions of the *b*- and *c*-axes predicted the detailed information concerning uniplanner orientation of benzene rings parallel to the film surface.
[DOI 10.1295/polymj.36.394]

KEY WORDS The Three Principal Crystallographic Axes / Poly(ethylene terephthalate) / Simultaneous Biaxial Stretching / Orientation Distribution Function of Crystallites / Benzene Rings /

The evaluation concerning molecular orientation was first proposed by Herman in terms of the second order orientation factor.[1] This factor is a sort of the second moment of the orientation function. After then, the orientation of crystallites was estimated by Roe and Krigbaum[2–4] in terms of the distribution function. The mathematical representation was given by an expansion of the distribution function in a series of generalized spherical harmonics. This method has been very important to obtain the orientation of the three principal crystallographic axes, the *a*-, *b*-, and *c*-axes, in terms of the orientation distribution function. Actually, there are several papers for estimating orientation distribution functions of the three principal crystallographic axes, the *a*-, *b*-, and *c*-axes of polyethylene,[5,6] poly(vinyl alcohol),[7,8] nylon 6[9] and cellulose.[10]

The first trial for poly(ethylene terephthalate) by Krigbaum and Balta[11] was done by using a simple uniaxially stretched films but their trial was absolutely unsuccessful. However, the recent development of computer program and high power X-Ray source provide easy peak separation of overlapped peaks and the orientation functions for the reciprocal lattice vectors can be obtained for a number of crystal planes with high accuracy. Consequently it becomes possible to calculate the orientation distribution functions of crystallites as well as of the *a*-, *b*-, and *c*-axes from the observed orientation functions of the reciprocal lattice vectors of the crystal planes. In previous paper,[12] the orientation of crystallites with a triclinic unit was evaluated in terms of orientation distribution function for a PBT film elongated uniaxially. The orientation distribution function of crystallites was calculated by using the functions of the reciprocal lattice vectors of 13 crystal planes. The successful results predicted that the preferential orientation function of the *c*-axis with respect to the stretching direction follows a floating model associated with an affine fashion.

This paper is concerned with the estimation for orientation distribution functions of the three pricipal crystallographic axes, the *a*-, *b*- and *c*-axes as well as the orientation function of crystallites, of a PET film elongated biaxially up to four-fold ($4 \times 4$), since PET films have been utilized as a commercial films because of good thermal dimensional stability and high Young's modulus. In this system, crystallites are oriented randomly around the film thickness direction and the uniplanner orientation of benzene rings parallel to the film surface provides good thermal dimensional stability and high Young's modulus. In spite of the important information, there has been no refine paper for the orientation of crystallites of PET. One is due to a complicated experimental procedure of this system in comparison with an uniaxially stretching film and the other is due to lower crystallinity. Accordingly, as a trial, the orientation of PET crystallites is estimated in terms of the orientation dis-

†To whom correspondence should be addressed (Fax: +81-742-20-3462, E-mail: m-matsuo@cc.nara-un.ac.jp).

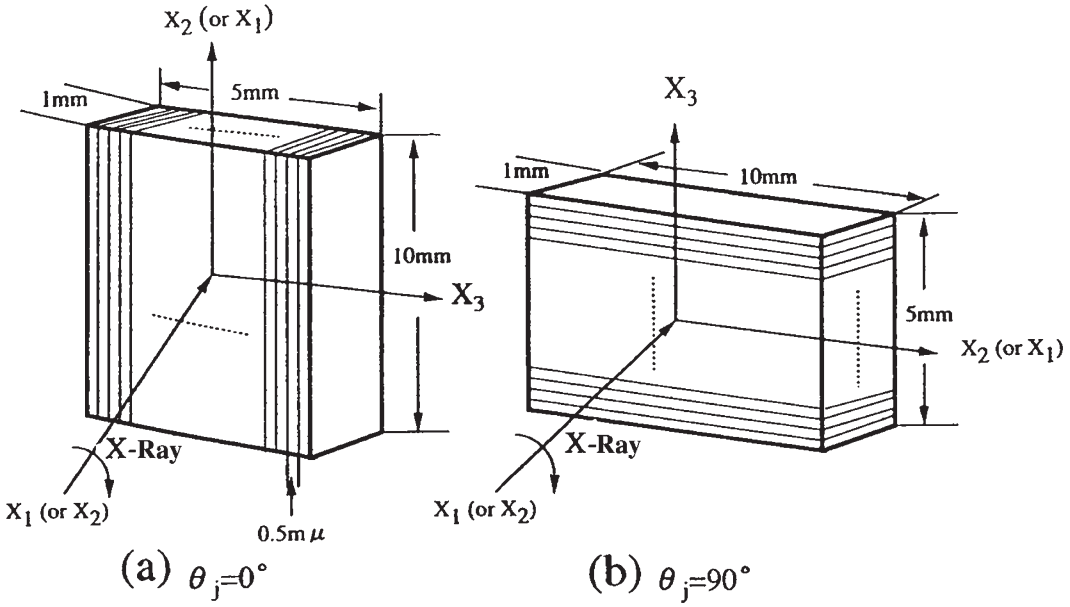


**Figure 1.** A number of thin stacked films to measure X-Ray diffraction intensity distribution as a dfunction of twoce the Bragg angle at (a) $\theta_j = 0^\circ$ (b) $\theta_j = 90^\circ$.

tribution function by using a simultaneous biaxial stretching film.

## EXPERIMENTAL

Samples used in this experiment were prepared from amorphous PET films furnished by courtesy of the Film Division Toyobo Co., Ltd. The film thickness is about 220 μm. The films was cut into strips of $90 \times 90$ mm. The specimen was held at 90 °C for 5 min and elongated biaxially to 4 folds ($4 \times 4$) using an Iwamoto biaxial stretcher. The draw ratio was determined in the usual way by measuring the displacement of ink marks placed $5 \times 5$ mm apart on the specimen prior to drawing. After stretching, the sample fixed in the stretcher was annealed at 150 °C for 10 min to promote inner-stress relaxation and removed from the stretcher.

Densities of PET films were measured by a pycnometer. A mixture of ethanol and carbon tetrachloride was used as a medium. The film was cut into fragments. The fragments were immersed in ethanol with ultrasonic washing for 30 min and subsequently vacuum-dried for 1 d. The weight percentage crystallinity was calculated by assuming the intrinsic densities of the crystal and amorphous regions to be 1.455 and 1.335 g/cm$^3$ respectively and the value was 47.1%.

The X-Ray measurements were carried out with a 12 kW rotating-anode X-Ray generator (Rigaku RDA-rA) operated at 200 mA and 40 kV. Here we must emphasize that the orientation function of the reciprocal lattice vector for many crystal planes with respect to the film normal direction cannot be obtained by using usual X-Ray diffraction technique for the thin films (<20 μm), since the number of crystallites within the irradiated area of X-Ray beam is too few to obtain strong X-Ray diffraction intensity. Then, the orientation distribution functions were measured only for the reciprocal lattice vectors of crystal planes with very strong diffraction intensity by using a pole figure attachment.[14] To obtain the orientation function of crystallites, however, we developed a small exquisite instrument to stack a number of thin films as shown in Figure 1. In such a stacked condition, measurements of the X-Ray diffraction intensity distribution could be performed using a horizontal scanning type monometer, operating at a fixed time step scan of 0.1°/40 s over a range of twice the Bragg angle $\theta_B$ from 7 to 55° by rotating about the stretching direction at 2–5° intervals of $\theta_j$ from 0 to 90°. The intensity distribution was measured as a function of a given rotational angle $\theta_j$. $\theta_j$ in Figure 1(a) and (b) correspond to 0° and 90°, respectively. For example, at $\theta_j = 0^\circ$, the diffraction intensity from the crystal plane parallel to the film surface becomes maximum, while at $\theta_j = 90^\circ$, the diffraction intensity from the crystal plane perpendicular to the film surface becomes maximum. Corrections of X-Ray diffraction intensity were made for air scattering, background noise, polarization, absorption, incoherent scattering and amorphous contribution. The intensity curve thus obtained was assumed to be due to the contribution of the intensity from the crystalline phase. The intensity curve $I_{cry}(2\theta_B)$ was separated into the contribution from the individual crystal planes, assuming that each peak had a symmetric form given by a Lorenzian function of in Eq 1, where $I_j^0$ is the maximum intensity of the $j$-th peak.

$$I_{\mathrm{cry}}(\theta_{\mathrm{B}},\theta_j)=\sum_j \frac{I_j^0}{1+(2\theta_0^j-2\theta_{\mathrm{B}})^2/\beta_j^2} \qquad (1)$$

Here $\beta_j$ is the half-width of the $j$-th peak at half the peak intensity and $2\theta_0^j$ is twice the Bragg angle at which the maximum intensity of the $j$-th peak appears. Using the same process at a given $\theta_j$ in the range from 0 to 90°, the intensity distribution $I_j(2\theta_{\mathrm{B}})$ can be determined for the respective $j$-th plane after integrating $I_{\mathrm{cry}}(2\theta_{\mathrm{B}})$ by $2\theta_{\mathrm{B}}$ at each $\theta_j$, and consequently the orientation distribution function $2\pi q_j(\cos\theta_j)$ of the $j$-th reciprocal lattice vector may be given by

$$2\pi q_j(\cos\theta_j)=\frac{\int_{2\theta_1}^{2\theta_2} I_{\mathrm{cry}}(\theta_{\mathrm{B}},\theta_j)d\theta_{\mathrm{B}}}{\int_0^{\pi}\int_{2\theta_1}^{2\theta_2} I_{\mathrm{cry}}(\theta_{\mathrm{B}},\theta_j)d\theta_{\mathrm{B}}\sin\theta_j d\theta_j} \qquad (2)$$

where $\theta_1$ and $\theta_2$ are the Bragg angles at the two feet of an isolated diffraction peak after the peak separation. The orientation factor $F_{\ell 0}^j$ was expressed as

$$F_{\ell 0}^j=\int_0^{\pi} 2\pi q_j(\cos\theta_j)P_\ell(\cos\theta_j)d\theta_j \qquad (3)$$

Incidentally, the uniaixial orientation of crystallites with respect to the film normal direction was confirmed by X-Ray diffraction pattern (through view) showing circular diffraction rings.

## RESULTS AND DISCUSSION

Figure 2(a) shows Cartesian coordinate 0-$U_1U_2U_3$ fixed within a structural unit, with respect to another Cartesian coordinate 0-$X_1X_2X_3$ fixed in a bulk specimen. The $U_3$ axis may be taken along the $c$-axis but has random orientation around the $X_3$ axis along the film thickness direction in the present system. The elongation directions are along the $X_1$ and $X_2$ axes. The orientation of the structural unit within the space of the film specimen may be specified by using three Euler angles, $\phi$, $\theta$, and $\eta$. The angles $\theta$ and $\phi$, which define the orientation of $U_3$ axis of the unit within the space, are polar and azimuthal angles, respectively, and $\eta$ specifies the rotation of the unit around its own $U_3$ axis. Coordinates (b) and (c) show a given $j$-th axis $r_j$ within the unit, specified by the polar angle $\theta_j$ and the azimuthal angle $\phi_j$ with respect to the Cartesian coordinate 0-$X_1X_2X_3$ and specified by polar angle $\Theta_j$ and the azimuthal angle $\Phi_j$ with respect to the 0-$U_1U_2U_3$ of the unit. On simultaneous biaxial stretching, $\phi_j$ is random around the $X_3$ axis. The values of $\Theta_j$ and $\Phi_j$ are were calculated from a crystal unit cell proposed by Daubeny *et al.*[13] containing one chemical unit with $a=4.56$ Å, $b=5.94$ Å, $c=10.75$ Å, $\alpha=98.5°$, $\beta=118°$ and $\gamma=112°$. They are listed in Table I. Based on the geometrical arrangement, the crystal unit in the bulk specimen and the crystal unit are shown in Figure 3 to facilitate understanding.

For an uniaxial system around film normal direction, the orientation distribution function $\omega(\theta,\eta)$ of crystallites may be calculated from the orientation distribution function of the reciprocal lattice vector of the $j$-th plane. Namely, the orientation distribution function $\omega(\theta,\eta)$ for crystallites with a triclinic unit cell may be obtained by using the orientation factor $F_{\ell 0}^j$

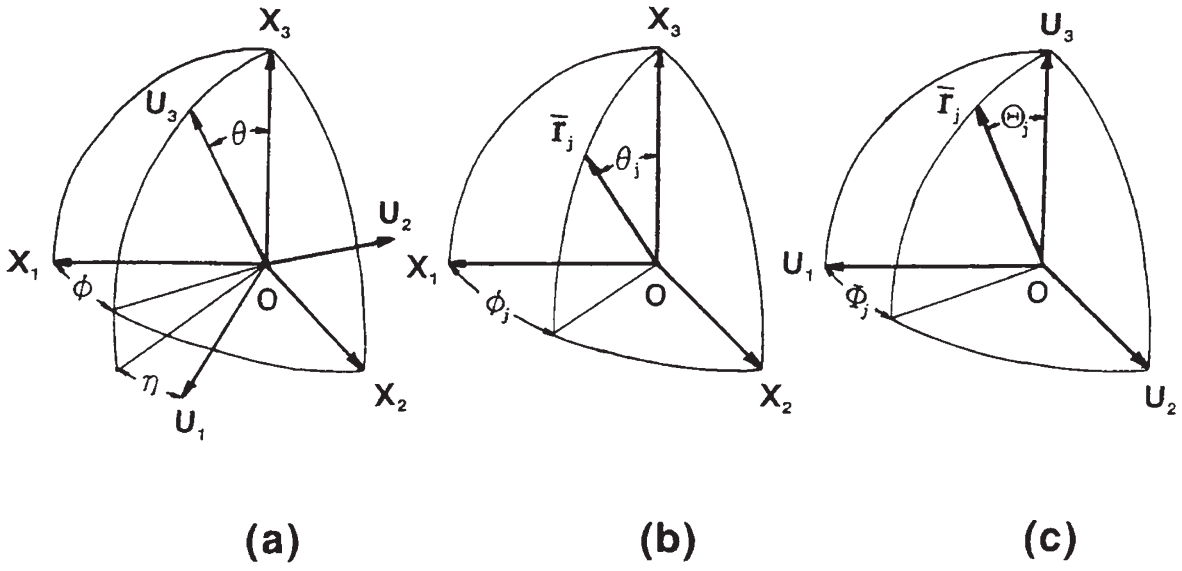


**Figure 2.** Cartesian coordinates illustrating the gometrical relation: (a) Euler angles $\theta$ and $\eta$ which specify the orientation of coordinate 0-$U_1U_2U_3$ of structural unit with respect to coordinate 0-$X_1X_2X_3$ of specimen, (b) Angles $\theta_j$ and $\phi_j$ which specify the orientation of the given $j$-th axis of the structural unit with respect to the coordinate 0-$X_1X_2X_3$, (c) Angles $\Theta_j$ and $\Phi_j$ which specify the orientation of $j$-th axis of the structural unit with respect to the coordinate 0-$U_1U_2U_3$.

**Table I.** Crystallographic data for all crystal planes normal contributing to the measured intensity

| *hkl* | $2\theta_B$ | $\Theta_j$ | $\Phi_j$ |
|---|---|---|---|
| $(0\bar{1}1)$ | 16.42 | 59.85 | 102.57 |
| (010) | 17.53 | 90.00 | 59.44 |
| $(\bar{1}11)$ | 21.31 | 67.18 | 123.59 |
| $(\bar{1}10)$ | 22.54 | 90.00 | 137.83 |
| (011) | 23.57 | 69.44 | 47.94 |
| $(\bar{1}12)$ | 24.71 | 47.91 | 105.96 |
| (100) | 25.69 | 90.00 | 0.00 |
| $(\bar{1}03)$ | 26.44 | 19.81 | 155.49 |
| $(1\bar{1}1)$ | 27.84 | 72.66 | 31.65 |
| $(0\bar{1}3)$ | 28.75 | 29.93 | 53.11 |
| (003) | 30.77 | 35.81 | 11.96 |
| $(11\bar{2})$ | 31.15 | 57.71 | 28.93 |
| $(1\bar{2}0)$ | 31.44 | 90.00 | 75.60 |
| (012) | 31.96 | 58.61 | 40.51 |
| $(\bar{1}\bar{1}3)$ | 32.44 | 39.62 | 146.20 |
| $(\bar{1}21)$ | 32.73 | 75.26 | 112.52 |
| $(\bar{1}2\bar{1})$ | 32.87 | 75.32 | 93.52 |
| $(0\bar{2}2)$ | 33.18 | 59.85 | 102.57 |
| $(1\bar{2}1)$ | 33.37 | 75.54 | 64.88 |
| $(\bar{1}05)$ | 42.67 | 9.77 | 60.20 |
| $(0\bar{2}4)$ | 42.73 | 38.07 | 77.80 |
| (111) | 45.27 | 79.26 | 22.05 |
| $(\bar{2}10)$ | 45.91 | 90.00 | 160.34 |
| $(\bar{1}\bar{2}4)$ | 47.32 | 44.38 | 128.54 |
| $(1\bar{3}2)$ | 48.31 | 69.48 | 76.24 |
| $(\bar{2}05)$ | 48.42 | 29.03 | 164.38 |
| $(\bar{1}31)$ | 49.06 | 80.05 | 81.46 |
| $(12\bar{1})$ | 49.50 | 80.13 | 37.61 |
| $(03\bar{2})$ | 49.66 | 70.03 | 109.42 |
| *a*-axis | | 118.00 | 329.44 |
| *b*-axis | | 98.50 | 90.00 |
| *c*-axis | | 0.00 | 0.00 |
| $c^*$-axis | | 5.00 | 90.00 |

obtained experimentally (see Eq 3) in accordance with the previous paper,[12] which are given by Daubeny *et al.*[13]

$$F_{\ell 0}^{j} = F_{\ell 00}P_{\ell}(\cos\Theta_j) + 2\sum_{n=1}^{\ell}\frac{(\ell-n)!}{(\ell+n)!} \times (F_{\ell 0n}\cos n\Phi_j - G_{\ell 0n}\sin n\Phi_j)P_{\ell}^{n}(\cos\Theta_j) \quad (4)$$

$$4\pi^2\omega(\theta,\eta) = \frac{1}{2} + 2\sum_{\ell=2}^{\infty}\left[\frac{2\ell+1}{2}\left\{F_{\ell 00}P_{\ell}(\xi) + 2\sum_{n=1}^{\ell}\frac{(\ell-n)!}{(\ell+n)!}(F_{\ell 0n}\cos n\eta + G_{\ell 0n}\sin n\eta)P_{\ell}^{n}(\xi)\right\}\right] \quad (5)$$

and

$$2\pi q_j(\cos\theta_j) = \frac{1}{2} + 2\sum_{\ell=2}^{\infty}\frac{2\ell+1}{2}F_{\ell 0}^{j}P_{\ell}(\xi_j) \quad (6)$$

In actual estimation of the orientation distribution function of crystallites, we must consider the difficulty of peak separation by Eq 1. Namely, there are some crystal planes whose Bragg angle reflections are located very close to each other. Especially, the separation is extremely difficult for crystal planes with weak diffraction intensity. The individual functions $2\pi q_j(\cos\theta_j)$ can be obtained clearly for the crystal planes with strong diffraction intensity, while the other functions must be estimated as a overlapped peak of two or three crystal planes. In this case, the composed function $q_j(\cos\theta_j)$ includes the contribution of several

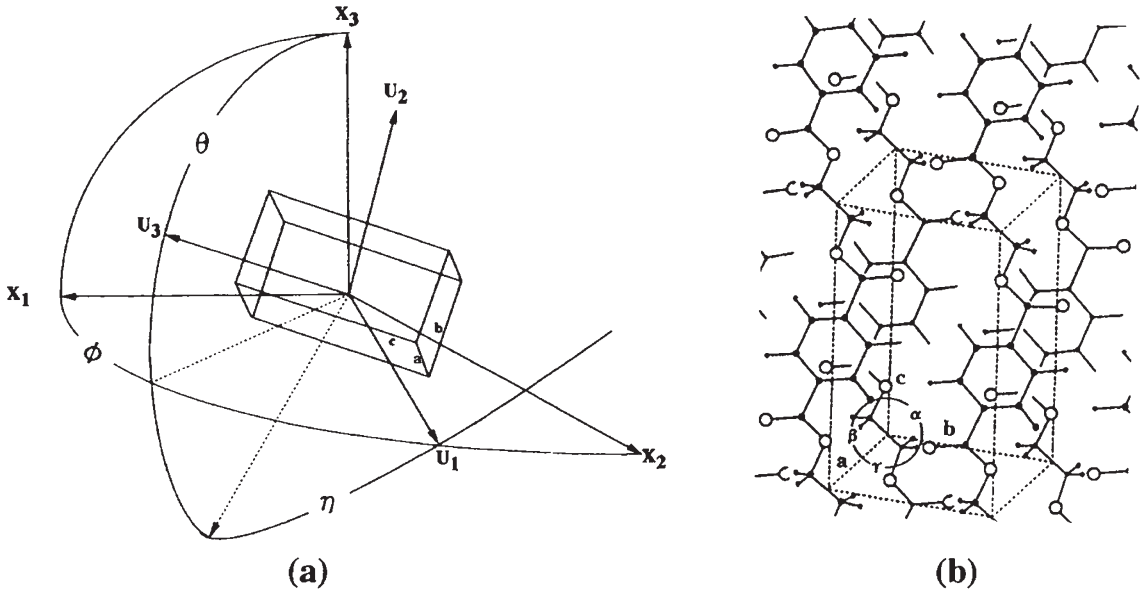


**Figure 3.** Geometrical arrangement of the crystal unit of PET and the schematic diagram of the unit cell.

planes as follows:

$$2\pi q_j(\cos\theta_j) = 2\pi \sum_{i=1}^{Ni} C_{ji} q_{ji}(\cos\theta_j) \tag{7}$$

The concept underlying Eq 7 was first presented by Roe and Krigbaum.[2,3] $N_j$ is the number of the $j$-th superposed peak and $C_{ji}$ is the relative (normalized) weight for the vector $\boldsymbol{r}_{ji}$. Before the numerical calculation by computer, initial values of $C_{ji}$ are given by

$$C_{ji} = \frac{F_{ji}}{\sum_{i=1}^{N_i} F_{ji}} \tag{8}$$

where $F_{ji}$ is the structure factor of the $j$-th crystal plane.

In this case, Eq 4 may be rewritten as follows:

$$F^j_{\ell 0} = F_{\ell 00} \sum_{i=1}^{N_i} C_{ji} P_\ell(\cos\Theta_j) + 2 \sum_{n=1}^{\ell} \frac{(\ell-n)!}{(\ell+n)!} \times \left( F_{\ell 0n} \sum_{i=1}^{N_i} C_{ji} P^n_\ell(\cos\Theta_{ji}) \cos n\Phi_{ji} - G_{\ell 0n} \sum_{i=1}^{N_i} C_{ji} P^n_\ell(\cos\Theta_{ji}) \sin n\Phi_{ji} \right) \tag{9}$$

In preliminary experiment, the series expansion up to $\ell = 14$ is confirmed to be enough to realize good fitting even for $2\pi q_j(\cos\theta_j)$ of the (100) plane with the sharpest profile among all crystal planes observed. In doing so, $2\pi q_j(\cos\theta_j)$ was calculated by a series expansion using Eq 6 and the calculated curve was compared with the experimental curve obtained by Eq 2. This indicates that in PET crystallites with a triclinic unit, the $j$-th orientation factors $F^j_{\ell 0}$ must be obtained for 29 crystal planes.

As a first step, the generalized orientation factors, $F_{\ell 0n}$ and $G_{\ell 0n}$ must be determined by solving Eq 9 using a least-square method. In doing so, the needed values of $\Theta_j$ and $\Phi_j$ can be obtained from a crystal unit of PET and are listed in Table I, which were calculated by a crystal unit cell proposed by Daubeny *et al.*[13] Thus, $F^j_{\ell 0}$ calculated from $F_{\ell 0n}$ and $G_{\ell 0n}$ by Eq 9 lead to $2\pi q_j(\cos\theta_j)$ by using Eq 6 or 7. The resulting calculated curves must be in good agreement with those from Eq 2 obtained experimentally by X-Ray diffraction measurements. Namely, one must confirm the accuracy of the experimental data. For this purpose, weighting factors $\rho_j$ were assumed initially to be nearly proportional to square of the structure factor and were subsequently varied to obtain the best fit between experimental and calculated results by the simplex method.[15] In actual calculation by computer, $\rho_j$ is fixed to be unity for the (100) plane with the strongest diffraction intensity. A mean-square error $R$ between the calculated factor $(F^j_{\ell 0})_{\mathrm{cal}}$ and recalculated factor $(F^j_{\ell 0})_{\mathrm{recal}}$ was obtained using:

$$R = \frac{\sum_j \sum_\ell \rho_j \left[ (F^j_{\ell 0})_{\mathrm{cal}} - (F^j_{\ell 0})_{\mathrm{recal}} \right]}{\sum_j \sum_\ell \rho_j \left[ (F^j_{\ell 0})_{\mathrm{cal}} \right]} \tag{10}$$

As described above, we recalculated $F^j_{\ell 0}$, in turn, from the values of $F_{\ell 0n}$, and $G_{\ell 0n}$ assuring the minimized value of $R$ in Eq 10 by best fitting of $\rho_j$ and further calculated $2\pi q_j(\cos\theta_j)$. The computer simulation provided very small values of $\rho_j$ for the less accuracy crystal planes with weak diffraction intensity to give the best fit between calculated and observe $2\pi q_j(\cos\theta_j)$ for crystal planes with high X-Ray diffraction intensity. This technique is very important. If the crystal planes with weak diffraction intensity are eliminated to solve Eq 9, termination error of the spherical harmonics due to fewer expansion by $\ell$ provides such serious result that no crystal plane gives the good fit between observed and recalculated functions. The value of $R$ in Eq 10 was 9.3% in the present case. The values of $\rho_j$ are listed in Table II. As the re-

**Table II.** Weight Parameters $\rho_j$ and $C_{ij}$ as well as the second order orientation factor observed for the crystal planes

| $i$ | $2\theta$ | $hkl$ | $\rho_j$ | $C_{ij}$ | $F^j_{20}$ |
|---|---|---|---|---|---|
| 1 | 16.42 | $(0\bar{1}1)$ | 0.73793 | | −0.200 |
| 2 | 17.53 | (010) | 0.50035 | | −0.107 |
| 3 | 21.31 | $(\bar{1}11)$ | 0.43793 | | 0.0743 |
| 4 | 22.54 | $(\bar{1}10)$ | 0.00959 | | 0.411 |
| 5 | 23.57 | (011) | 0.21451 | | 0.0124 |
| 6 | 24.71 | $(\bar{1}12)$ | 0.39700 | | −0.269 |
| 7 | 25.69 | (100) | 1.00000 | | 0.605 |
| 8 | 26.44 | $(\bar{1}03)$ | 0.09775 | | −0.407 |
| 9 | 27.84 | $(1\bar{1}1)$ | 0.07939 | | 0.470 |
| 10 | 28.75 | $(0\bar{1}3)$ | 0.19120 | | −0.357 |
| 11 | 30.77 | (003) | 0.27201 | | −0.106 |
| 12 | 31.44 | $(11\bar{2})$ | 0.10076 | 0.1818 | 0.706 |
| | | $(1\bar{2}0)$ | | 0.4091 | −0.0053 |
| | | (012) | | 0.4091 | 0.0042 |
| 13 | 32.80 | $(\bar{1}\bar{1}3)$ | 0.29521 | 0.2713 | −0.205 |
| | | $(\bar{1}21)$ | | 0.4722 | −0.116 |
| | | $(\bar{1}2\bar{1})$ | | 0.2565 | −0.141 |
| 14 | 33.28 | $(0\bar{2}2)$ | 0.15239 | 0.9417 | −0.200 |
| | | $(1\bar{2}1)$ | | 0.0583 | 0.107 |
| 15 | 42.70 | $(\bar{1}05)$ | 0.41677 | 0.0092 | −0.483 |
| | | $(0\bar{2}4)$ | | 0.9918 | −0.267 |
| 16 | 45.58 | (111) | 0.33893 | 0.0795 | 0.394 |
| | | $(\bar{2}10)$ | | 0.9205 | 0.607 |
| 17 | 47.38 | $(\bar{1}\bar{2}4)$ | 0.000403 | | −0.233 |
| 18 | 48.45 | $(1\bar{3}2)$ | 0.00256 | 0.5000 | −0.037 |
| | | $(\bar{2}05)$ | | 0.5000 | −0.282 |
| 19 | 49.55 | $(\bar{1}31)$ | 0.00206 | 0.5088 | −0.157 |
| | | $(12\bar{1})$ | | 0.2809 | 0.186 |
| | | $(03\bar{2})$ | | 0.2103 | −0.145 |

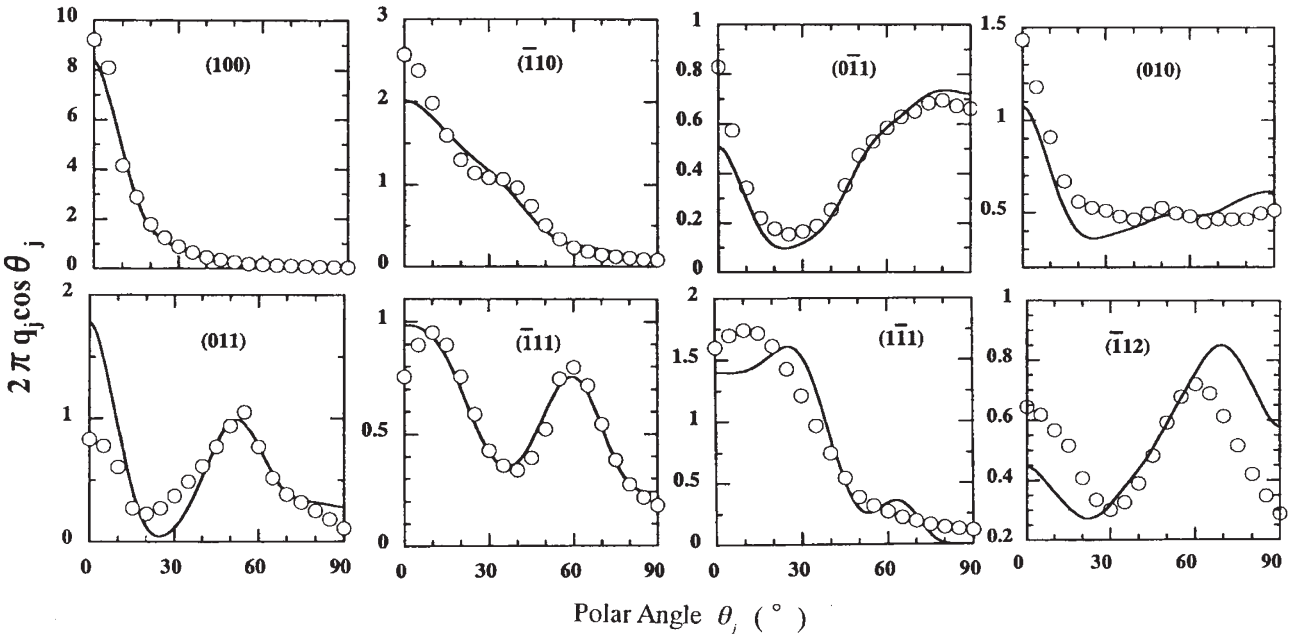


**Figure 4.** The observed orientation functions of $2\pi q_j(\cos\theta_j)$ (open circles) and the recalculated functions (solid curves) for the indicated crystal planes of a PET film drawn to $\lambda = 4$ biaxially.

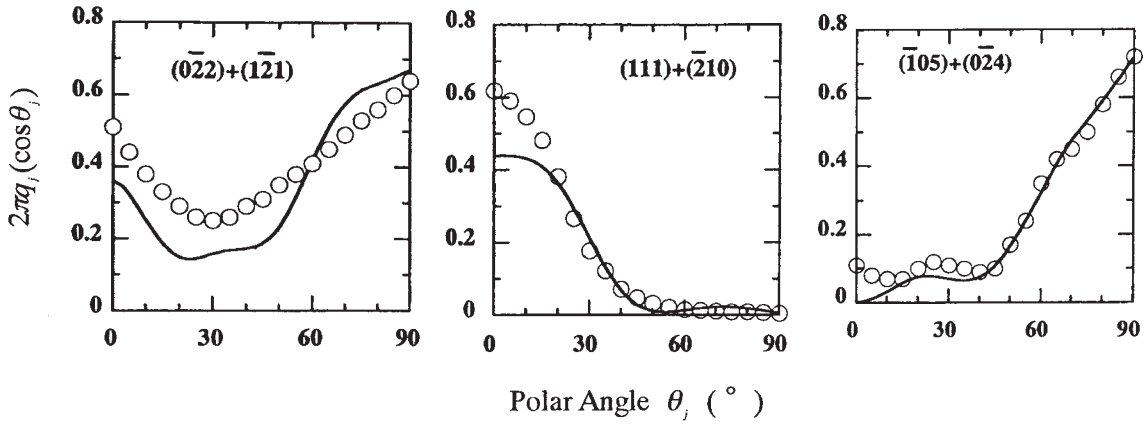


**Figure 5.** The observed orientation functions of $2\pi q_j(\cos\theta_j)$ (open circles) and the recalculated functions (solid curves) for the indicated superposed crystal planes of the PET film drawn to $\lambda = 4$ biaxially.

sults, the individual recalculated functions for 8 crystal planes give the good fit with the experimental functions and the superposed functions for 8 crystal planes are also the same tendency. The values of for the crystal planes with very weak diffraction intensity were much smaller than those of the other planes.

Figure 4 shows the observed orientation functions of $2\pi q_j(\cos\theta_j)$ (open circles) and the recalculated functions (solid curves) for the individual crystal planes. It is evident that good agreement between observed and recalculated distribution functions was observed, even for the less accurately crystal planes with lower weighting factors. The slight disagreement is due to the fact that there exist a number of less accurately crystal planes with weak diffraction intensity. As discussed before, the series expansion of the spherical harmonics up to $\ell = 14$ is enough to obtain good agreement between observed and recalculated results for the (100) plane with sharp distribution function of $2\pi q_j(\cos\theta_j)$.

Figure 5 shows the orientation functions of $2\pi q_j(\cos\theta_j)$ (open circles) and the recalculated functions (solid curves) obtained for overlapped peaks. In spite of less accurately crystal planes with lower weighting factors, fairly good agreement between observed and recalculated distribution functions was observed for 6 crystal planes. Such fairly good agreement is attributed to the computer development to determine the optimum values of $C_{ji}$ and $\rho_j$.

Figure 6 shows the orientation distribution function of crystallites $\omega(\theta, \eta)$ calculated using Eq 5 with the coefficients $F_{\ell 0n}$ and $G_{\ell 0n}$ determined from Eq 9 with $\ell$ limited to 14. As can be seen from this figure, the orientation distribution of PET crystallites is slightly

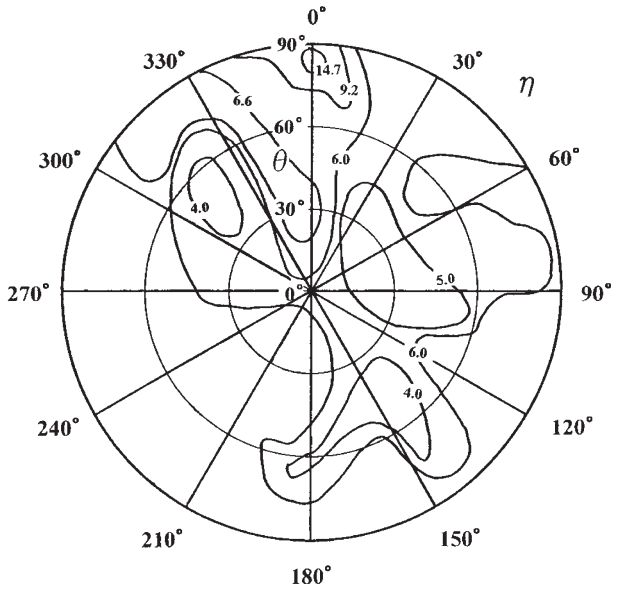


**Figure 6.** Orientation distribution function $\omega(\theta, \eta)$ of crystallites of the PET film drawn to $\lambda = 4$ biaxially.

complicated under simultaneous biaxially stretching. Namely, in the range of $\eta$ from 0 to 360°, $\omega(\theta, \eta)$ shows considerable dependence of $\eta$. The maximum population of $\omega(\theta, \eta)$ appears at $\theta = 85°$ and $\eta = 0$ indicating the most probable orientation of crystallites deviate 5° from the film surface. This is very important and such detailed information cannot be obtained from the second order orientation factor defined by Herman.[1] However, this is different from the analysis that the *c*-axis and the benzene rings are oriented parallel to the film surface. This shall be discussed later. Anyway, the population indicates the orientation of the crystallites is different from a floating model associated with affine mode. If orientation follows affine mode, the contour map with maximum population must show a circular profile independent of $\eta$. Namely, the considerable $\eta$-dependence in Figure 6 is due to the specific rotation of crystallites around the *c*-axis as has been observed for the orientation of crystallites of polyethylene films.[16] If $\omega(\theta, \eta)$ shows a circular contour map with a maximum peak at $\theta = 90°$, all $2\pi q_j(\cos\theta_j)$ of the $(hk0)$ planes must show the same curves indicating random orientation of crystallites around their *c*-axis.

The orientation distribution functions of the *a*-, *b*- and *c*-axes in addition to the $c^*$-axis perpendicular to *a*–*b* plane can be determined by substituting the values of $\Theta_j$ and $\Phi_j$ for each axis (listed in Table I) into Eq 4 and by using Eq 6. Figure 7 shows the results. The functions of the *c*-axis (and the $c^*$-axis) and the *b*-axis show the similar orientation with respect to the stretching direction. The function of the *c*-axis can be obtained by the integration of $\omega(\theta, \eta)$ by $\eta$. The functions of the *b*- and *c*-axes have two peaks, a large peak at $\theta_j = 90°$ and a small peak at $\theta_j = 0°$ indicating two rotational modes of crystallites around their *c*-axis. The large peak at $\theta_j = 90°$ predicts the preferential orientation of benze rings parallel to the film surface. The peak supports the preferential orientation of the distribution of the *b*-axis. However, another peak at $\theta_j = 0°$ indicates the orientation of benzene rings perpendicular to the film surface. Such behavior is abnormal, although the possi-

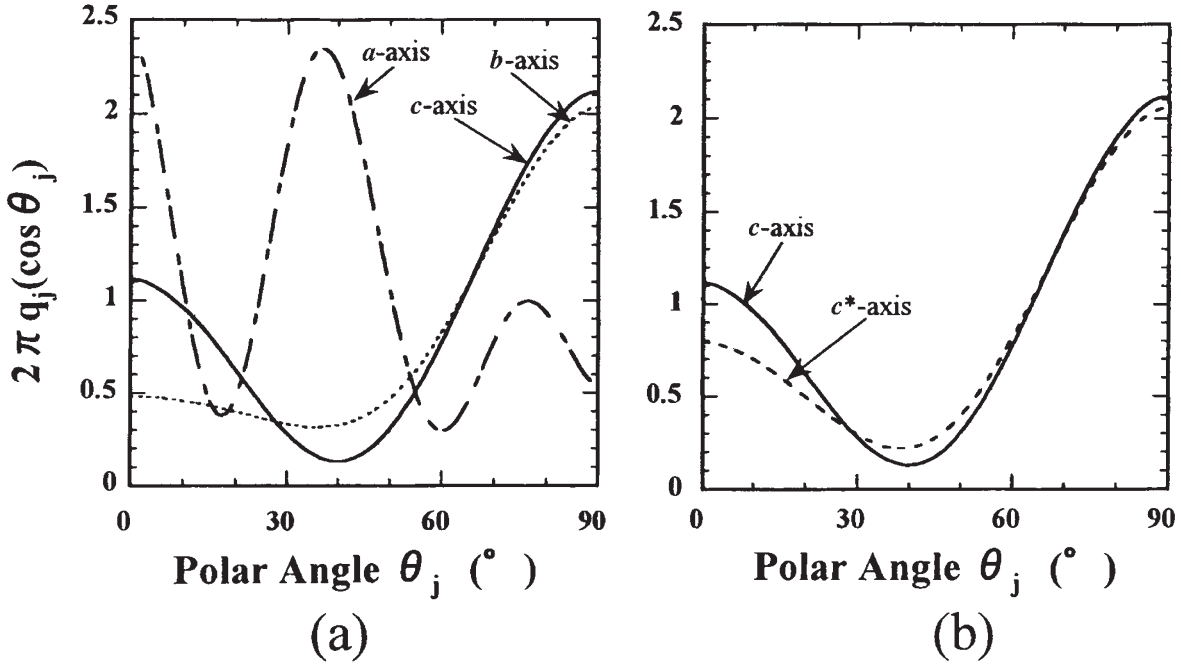


**Figure 7.** Orientation distribution functions of the *a*-, *b*- and *c*-axes in addition to the axis perpendicular to the *a*–*b* plane of the PET film drawn to $\lambda = 4$ biaxially.

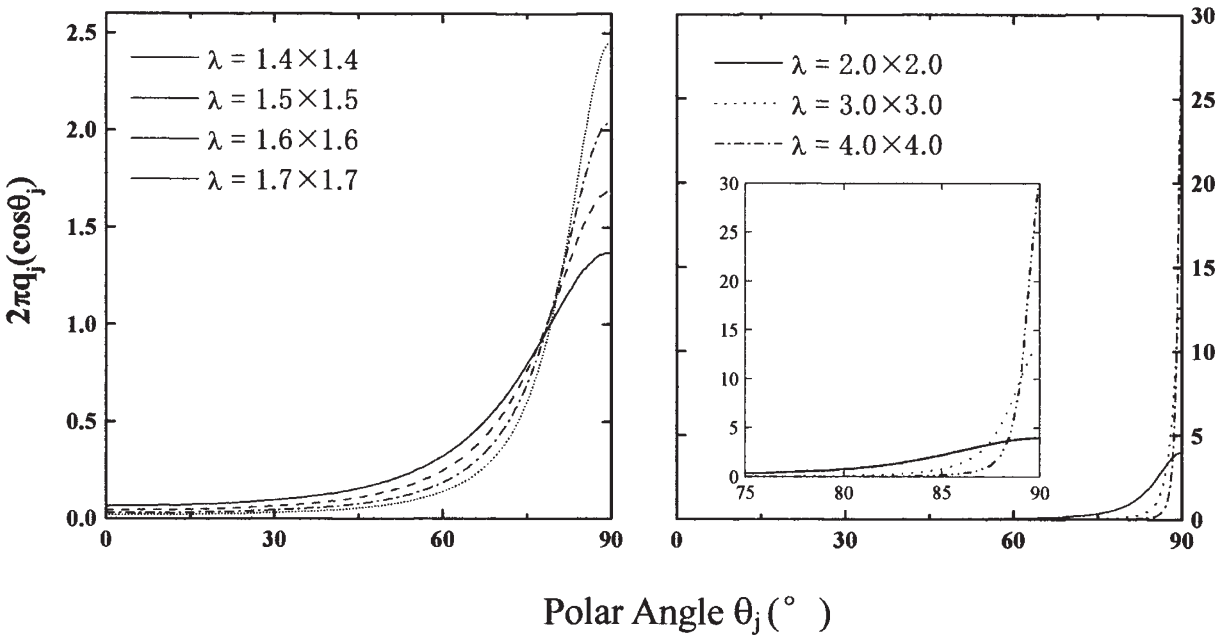


**Figure 8.** Orientation distribution function calculated by a floating model at the indicated $\lambda$ under simultaneous biaxially stretching.

bility is fewer. The orientation of the *a*-axis shows a very complicated curve having two peaks. The peak at $\theta_j = 0^\circ$ supports the orientation of benzene rings parallel to the film surface, while the peak at $\theta_j = 35^\circ$ is unresolved problem. Of course, such abnormal profile is not attributed to artifacts of expansion of $2\pi q_j(\cos\theta_j)$ into infinite series of spherical harmonics. This is probably though to be due to an unresolved peak appeared at $\theta_j = 0^\circ$ of the *c*-axis and the *b*-axis. Thus the orientation of PET crystallites within the film can be represented approximately as $\theta = 90^\circ$ and $\eta = 0^\circ$ in Figure 3.

Finally, we shall check whether the orientation of the *c*-axis follows an affine fashion given by the following equation:[17]

$$\omega(\theta) = \frac{\lambda^3}{2\left\{\left(\lambda^6 - 1\right)\cos^2\theta + 1\right\}^{3/2}} \qquad (11)$$

Figure 8 shows the results. The curves corresponding the distribution function of the *c*-axis or *c**-axis show a peak at $\theta_j = 90^\circ$ and the peak becomes shaper with increasing draw ratio of $\lambda$. It is seen that the function at $\lambda = 1.6$ is in good agreement with that of the *c*-axis shown in Figure 6. This indicates that the orientation of the *c*-axis deviates from a floating model associated with an affine mode. Namely, the orientation of the *c*-axis and draw ratio do not take a linear geometrical relationship in the simultaneous biaxially stretching of a PET film. A series of successful results to obtain orientation distribution of PET under simultaneous biaxial stretching is due to the development of computer. As discussed before, first trial was done by Krigbaum and Balta[11] for a simple uniaxial drawn PET film with high crystallinity but they ended in a failure because of lower power of X-Ray source and lower calculation speed of the computer. The good agreement between the experimental and recalculated curves in the present paper is due to accurate accumulation of X-Ray diffraction intensity by using a small exquisite instrument to stack a number of thin films shown in Figure 1. The estimation of orientation of crystallites in terms of distribution function shall propose a new information for investigating deformation mechanism of polymer films under manufacturing process.

## CONCLUSIONS

The orientation of crystallites with a triclinic unit was evaluated in terms of orientation distribution function and the numerical calculation was carried out for a PET film elongated biaxially. The orientation distribution function $\omega(\theta, \eta)$ of crystallites was calculated by using the functions of the reciprocal lattice vectors of 29 crystal planes. The functions of the reciprocal lattice vectors were recalculated from $\omega(\theta, \eta)$. The recalculated functions were fairly in good agreement with the observed ones. The orientation of three principal crystallographic axes, the *a*-, *b*- and *c*-axes, which can not be measured directly by X-Ray diffraction technique, was also evaluated in terms of the orientation distribution function. As the results, the orientation of the *c*-axis oriented predominantly parallel to the film surface and the benzene rings were also oriented in the same manner. The orientation function of the *a*-axis and the *b*-axis deviated a floating model because of characteristic rotation of crystallites around the *c*-axis. The characteristic rotation is

indispensable to cause the uniplaner orientation of the benzene rings.

## REFERENCES


1. P. H. Herman, "Physics and Chemistry of Cellulose Fibers," Elsevier, New York, N.Y., 1949, pp 255 and 393.
2. R. J. Roe and W. R. Krigbaum, *J. Chem. Phys.*, **40**, 2608 (1964).
3. W. R. Krigbaum and R. J. Roe, *J. Chem. Phys.*, **41**, 737 (1964).
4. R. J. Roe, *J. Appl. Phys.*, **36**, 2024 (1965).
5. K. Fujita, S. Suehiro, S. Nomura, and H. Kawai, *Polym. J.*, **11**, 331 (1982).
6. M. Matsuo and C. Xu, *Polymer*, **38**, 4311 (1997).
7. Y. Bin, Y. Tanabe, C. Nakabayashi, H. Kurose, and M. Matsuo, *Polymer*, **42**, 1183 (2001).
8. M. Matsuo, Y. Bin, and M. Nakano, *Polymer*, **42**, 4687 (2001).
9. M. Matsuo, R. Sato, N. Yanagida, and Y. Shimizu, *Polymer*, **33**, 1640 (1992).
10. M. Matsuo, C. Sawatari, Y. Iwai, and F. Ozaki, *Macromolecules*, **23**, 3266 (1990).
11. W. R. Krigbaum and Y. I. Balta, *J. Phys. Chem.*, **71**, 1770 (1967).
12. M. Matsuo, R. Adachi, Y. Bin, and T. Xu, *Macromolecules*, in press.
13. R. de Daubeny, C. W. Q. Bunn, and C. Brown, *Proc. R. Soc. London, Ser. A*, **226**, 531 (1954).
14. N. Yoshihara, A. Fukushima, Y. Watanabe, A. Nakai, S. Nomura, and H. Kawai, *Sen-i Gakkaishi*, **37**, 387 (1981).
15. W. Spendly, G. R. Hext, and F. R. Homsworth, *Technometrics*, **4**, 441 (1962).
16. T. Nakashima, C. Xu, Y. Bin, and M. Matsuo, *Polym. J.*, **33**, 54 (2001).
17. W. Kuhn and F. Grun, *Kolloid-Z.*, **101**, 248 (1942).